Electronic Supplementary Information (ESI)

Eosin-Y and Sulfur-Codoped g-C_3N_4 Composite for Photocatalytic Applications: Regeneration of NADH/NADPH and Oxidation of Sulfide to Sulfoxide

Pooja Singh,[a] Rajesh K. Yadav,[a,*] Krishna Kumar,[a] Yubin Lee,[b] Abhishek K. Gupta,[c] Kuldeep Kumar,[d] B. C. Yadav,[d] S. N. Singh,[e] D. K. Dwivedi,[c] Sang-Ho Nam,[b,f] Atul P. Singh,[g] & Tae Wu Kim,[b,f,*]

[a]Department of Chemistry and Environmental Science, Madan Mohan Malaviya University of Technology, Gorakhpur, U.P.,273010, India

[b]Department of Chemistry, Mokpo National University, Muan-gun, Jeollanam-do, 58554, Republic of Korea.

[c]Department of Physics and Material Science, Madan Mohan Malaviya University of Technology, Gorakhpur, U.P.,273010, India

[d]Department of Physics, Babasaheb Bhimrao Ambedkar University of Lucknow, U.P., 226025, India

[e]Department of Humanities and Management Science, Madan Mohan Malaviya University of Technology, Gorakhpur, U.P., 273010, India

[f]Spectrochemical Analysis Center for Organic & Inorganic Materials and Natural Products, Mokpo National University, Muan-gun, Jeollanam-do, 58554, Republic of Korea

[g]Department of Chemistry, Chandigarh University, Mohali, Punjab, 140413, India

Corresponding Author

[*]Rajesh K. Yadav: rajeshkr_yadav2003@yahoo.co.in

[*]Tae Wu Kim: twkim@mokpo.ac.kr

1. Synthesis of EY-S-g-C_3N_4 photocatalyst

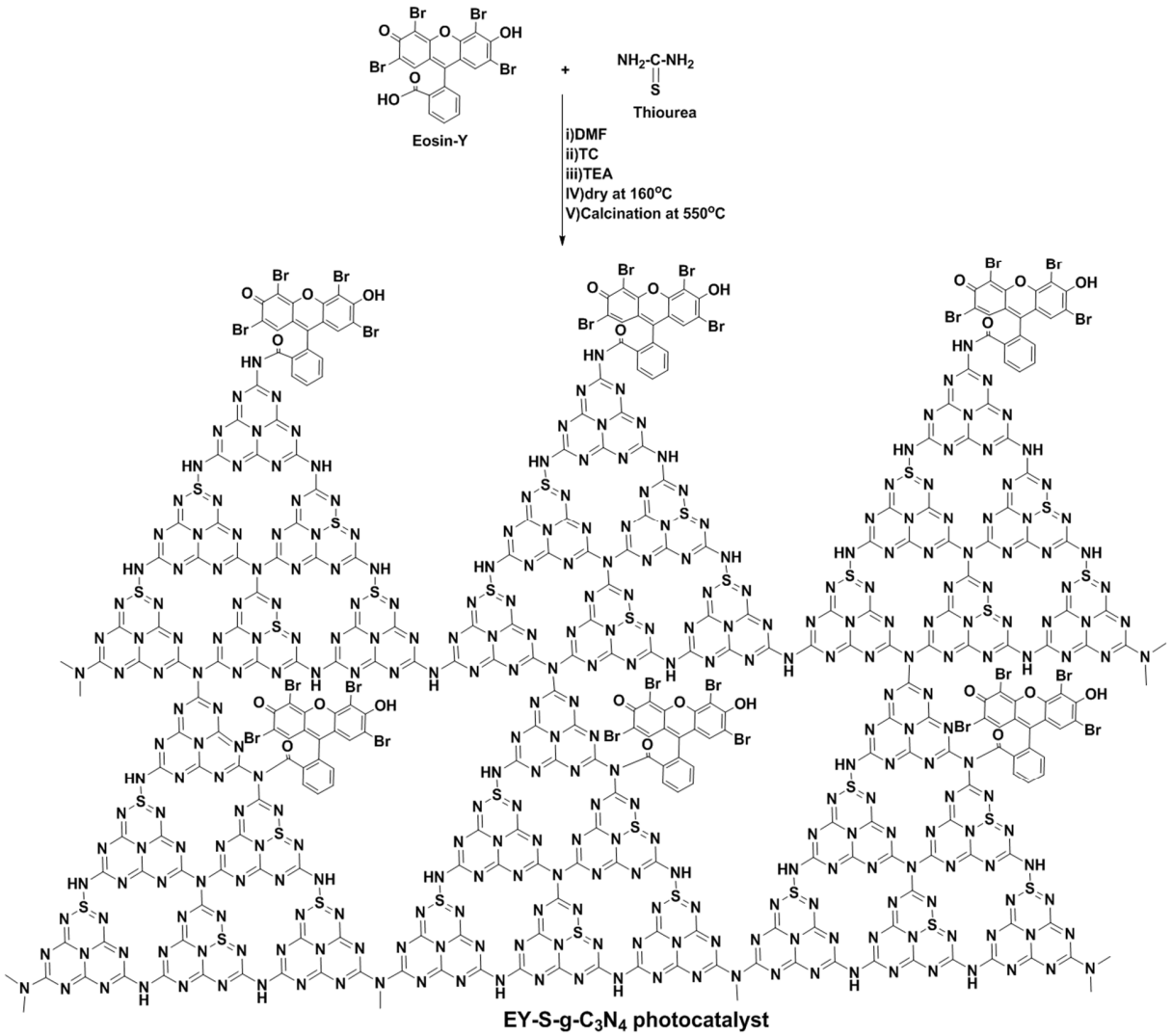

Figure S1. Synthesis of EY and sulfur-codoped EY-S-g-C_3N_4 photocatalyst.

2. Postulated reaction mechanism in the photoinduced regeneration of NAD(P)H

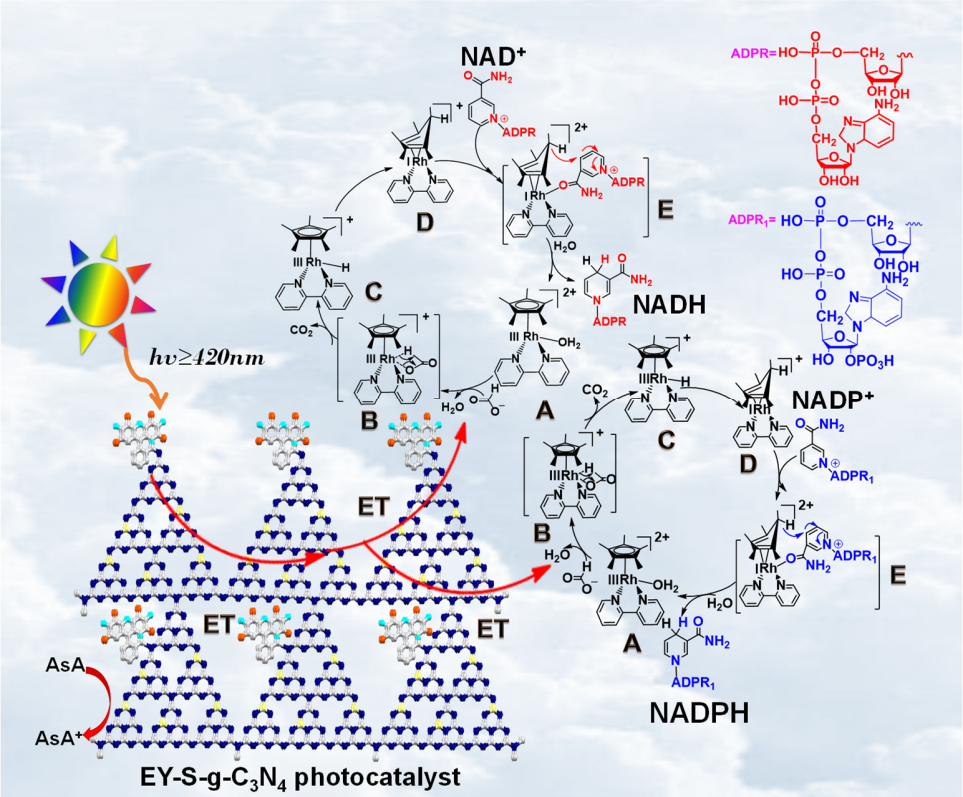

Figure S2. Pictorial representation of sequential electron transfers for the selective production of NAD(P)H. In this reaction, ADPR stands for adenosine diphosphate ribose and $ADPR_1$ indicates the derivative form of ADPR with one extra phosphate group.

3. Photocatalytic regeneration of 1,4-NAD(P)H investigated by the UV-visible spectroscopic measurements

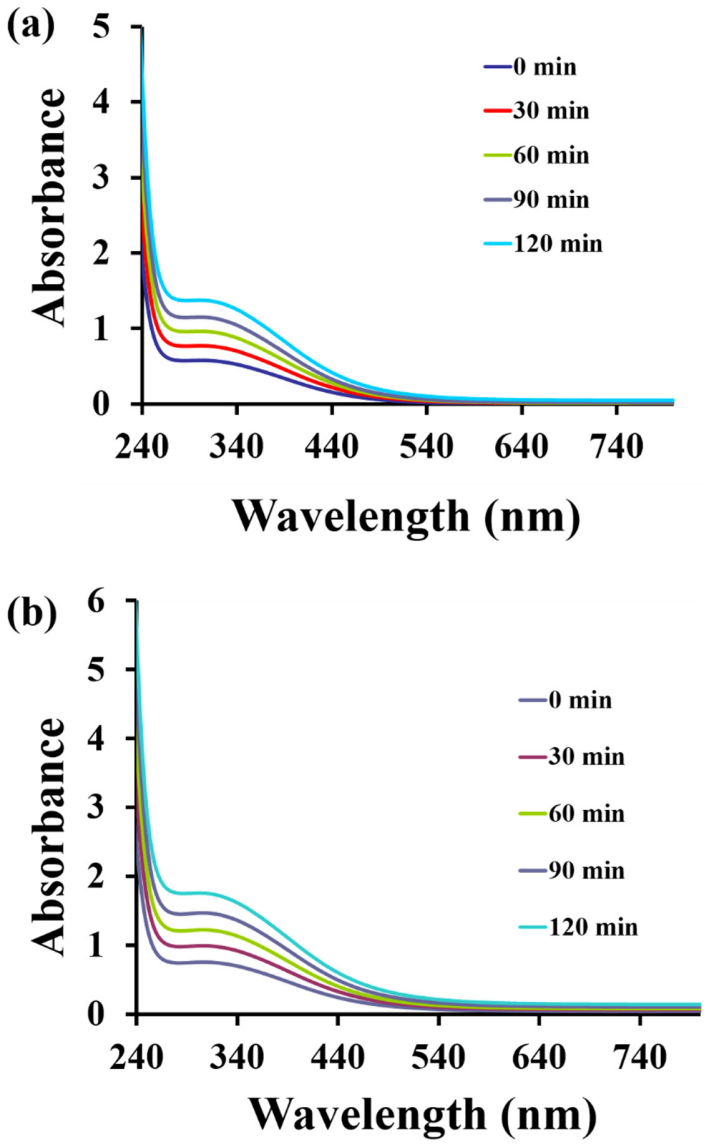

Figure S3. UV-visible spectra recorded for (a) NADH, and (b) NADPH regeneration as a function of reaction time during the irradiation of solar light. The reaction mixture contains 0.1 M phosphate buffer solution, 0.005 g EY-S-g-C_3N_4 photocatalyst, 0.2mM Rh-complex, 0.2 mM $NAD(P)^+$, and 0.1 M ascorbic acid (AsA) under the nitrogen-purged atmosphere at ambient temperature.

4. Reusability test for photocatalytic regeneration of NADH/NADPH from $NAD^+/NADP^+$

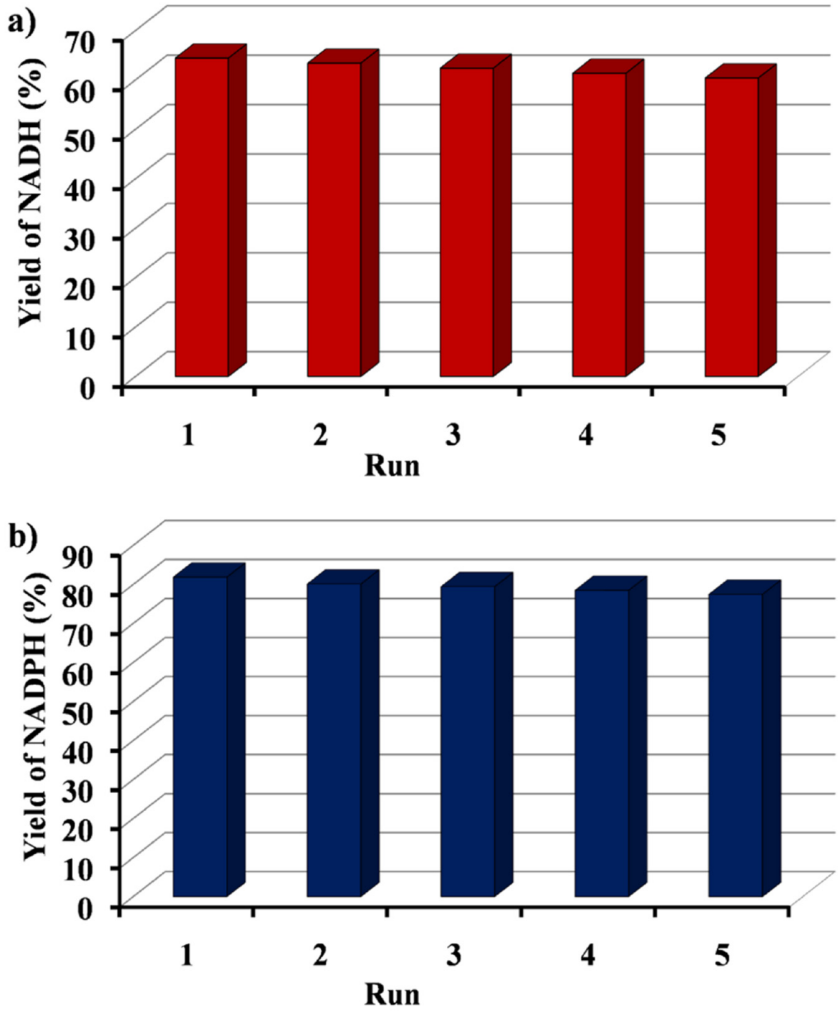

Figure S4. Reusability test (five times) with EY-S-g-C_3N_4 photocatalyst in solar-light-active photoregeneration of NADH (a), and NADPH (b) respectively. Reaction conditions: 2.3 mL sodium phosphate buffer (pH ~ 7.0, 0.1M), 0.005 g EY-S-g-C_3N_4 photocatalyst, 0.2mM of $NAD^+/NADP^+$, 0.2 mM of [Cp*Rh(bpy)Cl]Cl and ascorbic acid of 0.1 M under nitrogen atmosphere at ambient temperature (see details in experimental section of the manuscript). The reaction time for NADH/NADPH regeneration was set for 2 hours and yields were calculated for each run and shown here.

5. Reusability test for photocatalytic oxidation of sulfide to sulfoxide

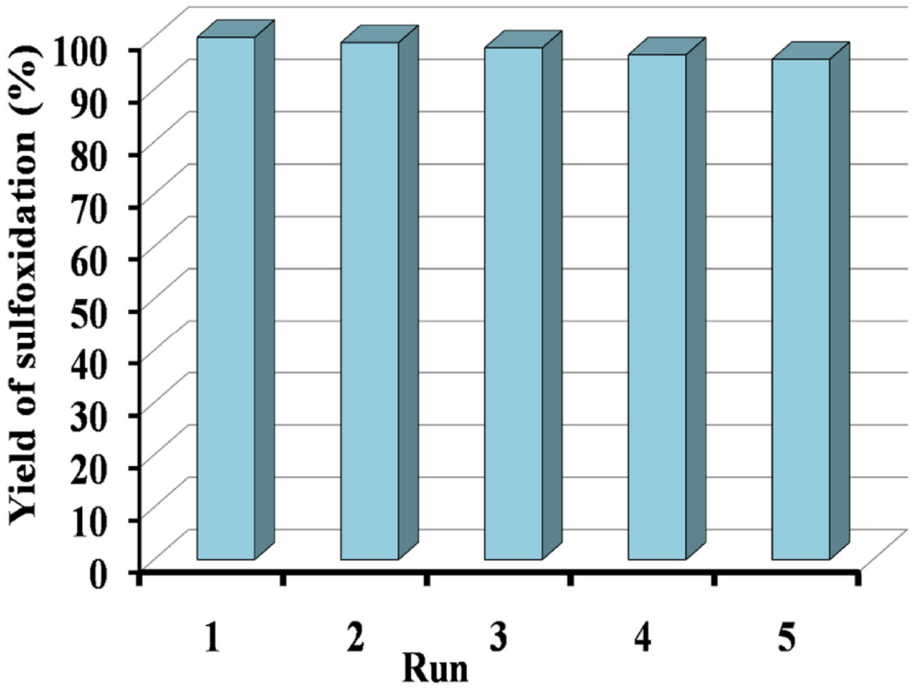

Figure S5. Reusability test of EY-S-g-C_3N_4 photocatalyst under solar-light irradiations for conversion of bis(4-chlorophenyl) sulfide to bis(4-chlorophenyl) sulfoxide.

6. Characterization of electronic transition using time-dependent density functional theory (TD-DFT)

First, we modelled the partial structure of EY-S-g-C_3N_4 including the 6 heptazine rings and one eosin-Y covalently linked with the terminal part of heptazine ring by employing density functional theory (DFT) calculation. Among the three different doping sites in g-C_3N_4, the local nitrogen (N) atoms, which atom is 2-fold coordinated with two carbon (C) atoms in C_6N_7 unit, were replaced by sulfur (S) atoms in order to form sulfur-dopedg-C_3N_4 structure. The molecular geometry of partial moiety of EY-S-g-C_3N_4 were optimized by using the level of B3LYP functional and 6-31G (d) basis set for all atoms. The vibrational frequencies of the optimized structure showed no imaginary vibrational frequencies, confirming that the optimized structure is in the stationary state. To obtain the information about the electronic transitions, we performed the time-dependent DFT calculation with the PBE0 functional and def2-SVP basis set because it has been known that PBE0 functional reasonably describes the absorption spectrum of sulfur-doped g-C_3N_4.[1] Since there are two different conformers in view of orientation of eosin-Y, we compared the electronic transitions for each conformer as shown in Fig. 5. All the DFT calculations were implemented by Gaussian 16 package.[2]

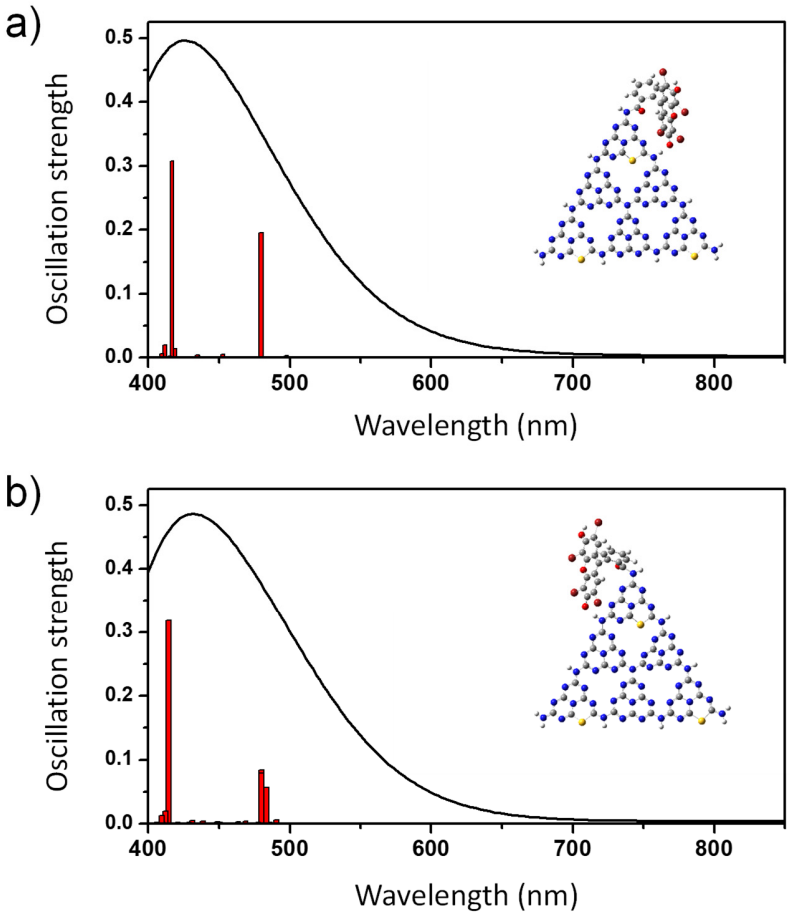

Figure S6. Absorption spectra of EY-S-g-C_3N_4 composite calculated from the two different conformational isomers. Theoretical absorption spectra (black line) of (a) conformational isomer with the eosin group located at the right side and (b) the other isomer with the eosin group located at the left side. The red-colored bars indicate the oscillation strengths at the certain wavelength. The theoretical absorption spectra were broadened by using the Gaussian convolution with the half-width of 0.330 eV.

7. Structural characteristic of as-synthesized S-g-C_3N_4

To characterize the as-synthesized S-g-C_3N_4, we performed the measurements by using power X-ray diffraction and photoluminescence spectroscopy. As shown in Fig. S7a, the data from the measurement of power X-ray diffraction (PXRD) shows the clear Bragg pattern around 27.0°, which corresponds to the interlayer stacking with the *d*-spacing of 3.28 Å. In the small-angle region, the peak around 13.0° is found and can be attributed to the characteristic graphitic structure of carbon nitride. In addition, we also measured the emission spectrum of S-g-C_3N_4 measured at the excitation of 350 nm by using Hitachi F4500 spectrophotometer shown in Fig. S7b. The emission spectrum shows the prominent peak around 440 nm, reflecting the existence of optical bandgap due to the incorporation of sulfur atoms to the graphitic carbon nitride.

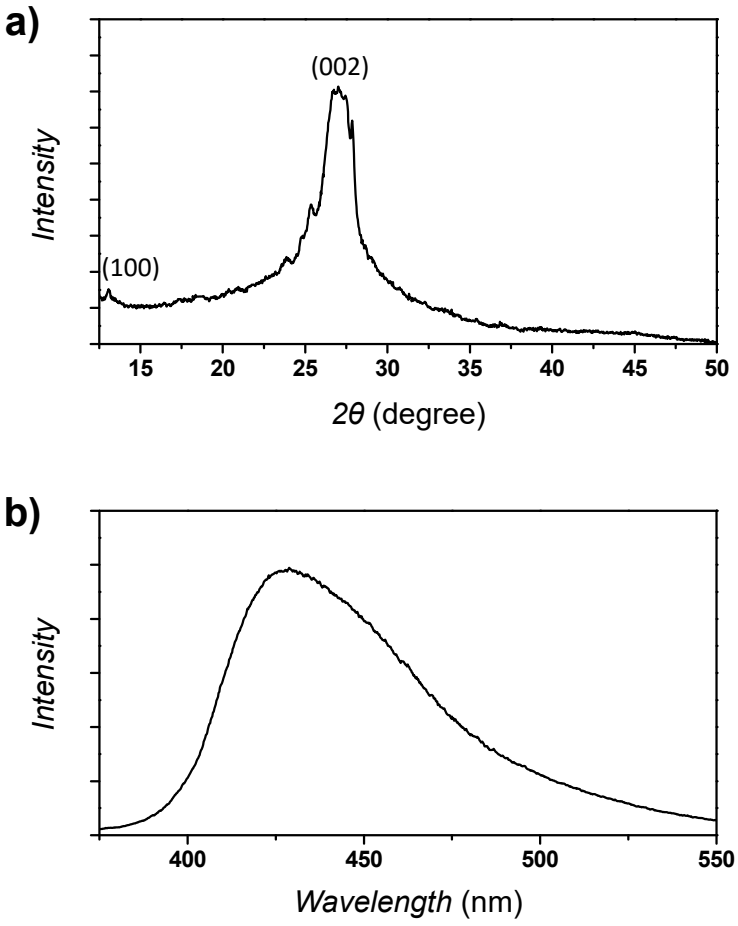

Figure S7. Characterization of sulfur-doped g-C_3N_4 by using powder X-ray diffraction (PXRD) and photoluminescence. (a) Results from the measurement of PXRD. (b) Emission spectrum measured at the excitation wavelength of 350 nm.

8. Characterization of structure of EY-S-g-C_3N_4 composite by using the solid-state ^{13}C NMR spectroscopy

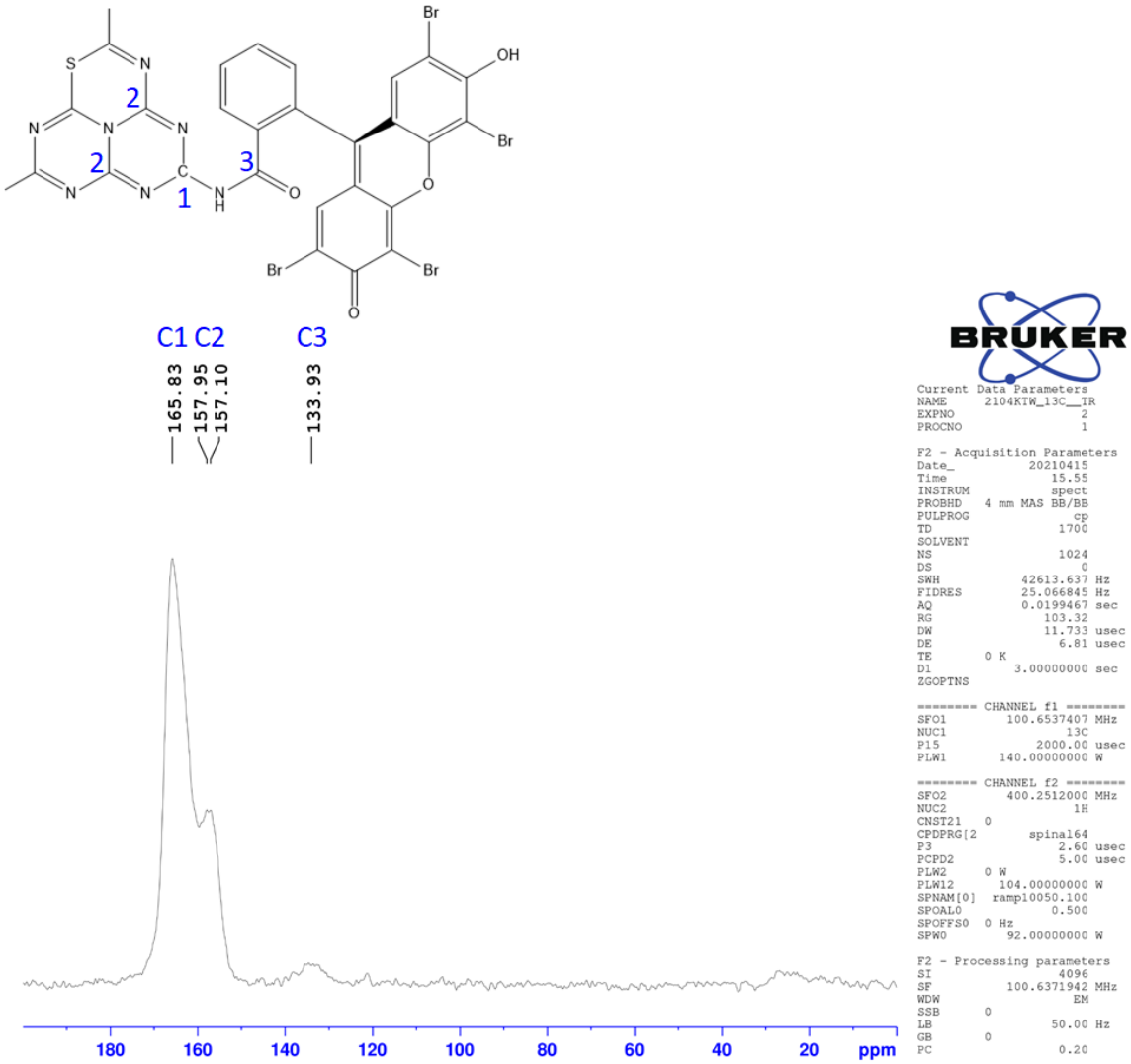

Figure S8. Cross-polarization magic angle spinning solid-state NMR spectrum of EY-S-g-C_3N_4 composite. The appearance of peak at 133.93 ppm can be attributed to the existence of ketonic carbon, which is formed by the covalent ligation between EY moieties and S-g-C_3N_4.

9. Synthesis and 1H NMR spectrum of rhodium complex

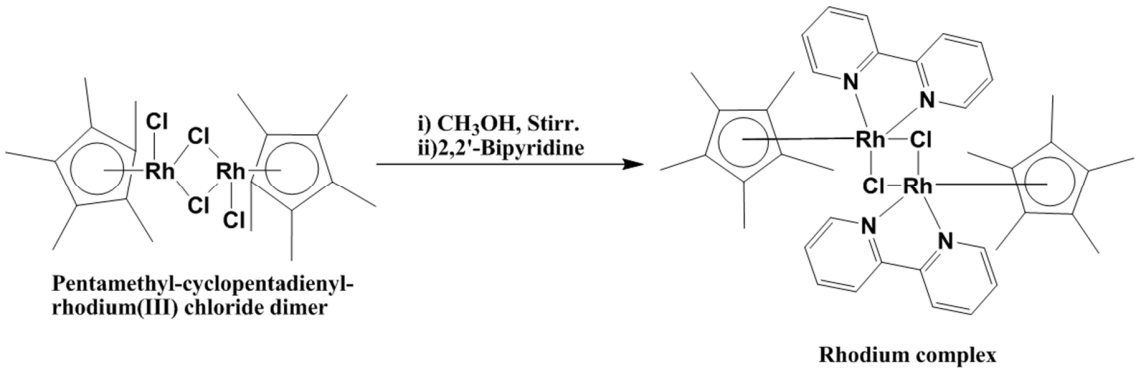

Figure S9. Synthesis of rhodium complex

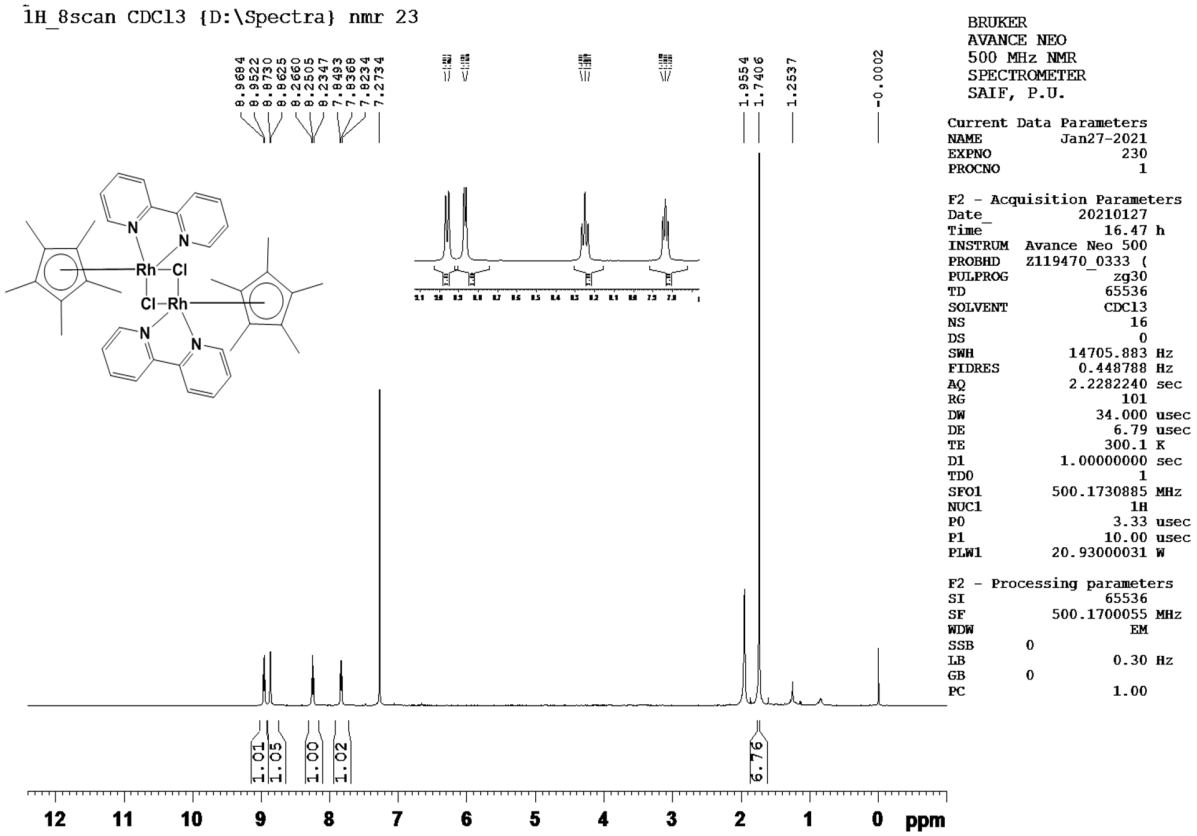

Figure S10. ^{1}H NMR spectrum of rhodium complex [Cp*Rh(bpy)Cl]Cl. ^{1}H NMR (500 MHz, $CDCl_3$) δ 1.74 (s,30H), 8.9 (d,4H), 8.8 (d,4H), 8.2 (t,4H), 7.8 (t,4H).

10. ^{1}H NMR spectra of bis(4-chlorophenyl) sulfoxide

The bis(4-chlorophenyl) sulfoxide product was prepared from bis(4-chlorophenyl) sulfide (1mmol, 0.255g), EY-S-g-C_3N_4 photocatalyst (0.005g), and 0.05 M HCl in 4 ml ethyl alcohol. The obtain product was purified by column chromatography (silica gel, ethyl acetate- hexane, 1:4).

^{1}H NMR(500 MHz, $CDCl_3$): δ 7.58-7.55 (d, J=15 Hz, 2H,ArH), 7.45-7.42 (d, J=15 Hz, 2H, ArH).

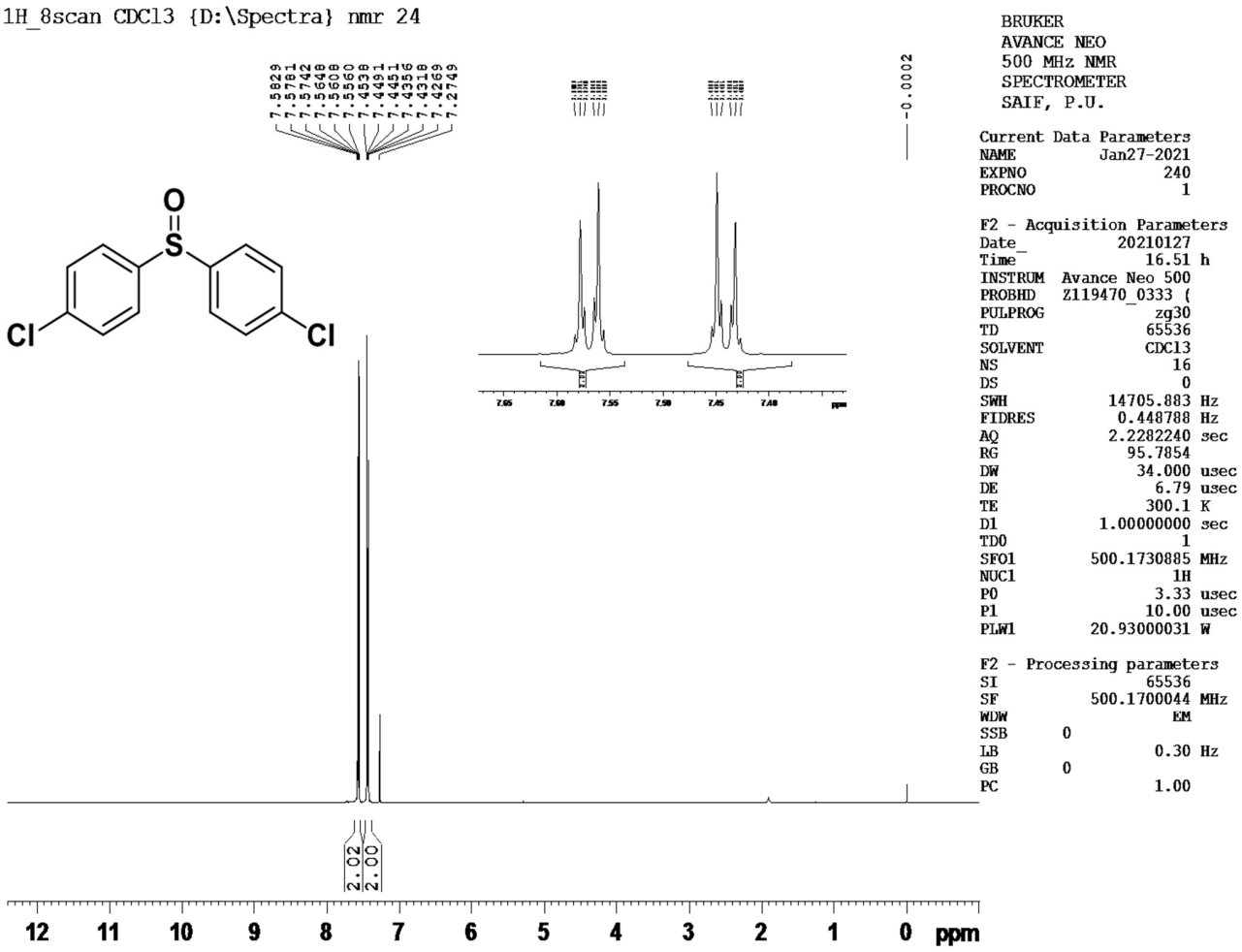

Figure S11. ^{1}H NMR spectrum of bis(4-chlorophenyl) sulfoxide

11. Mass spectra of bis (4-chlorophenyl) sulfoxide

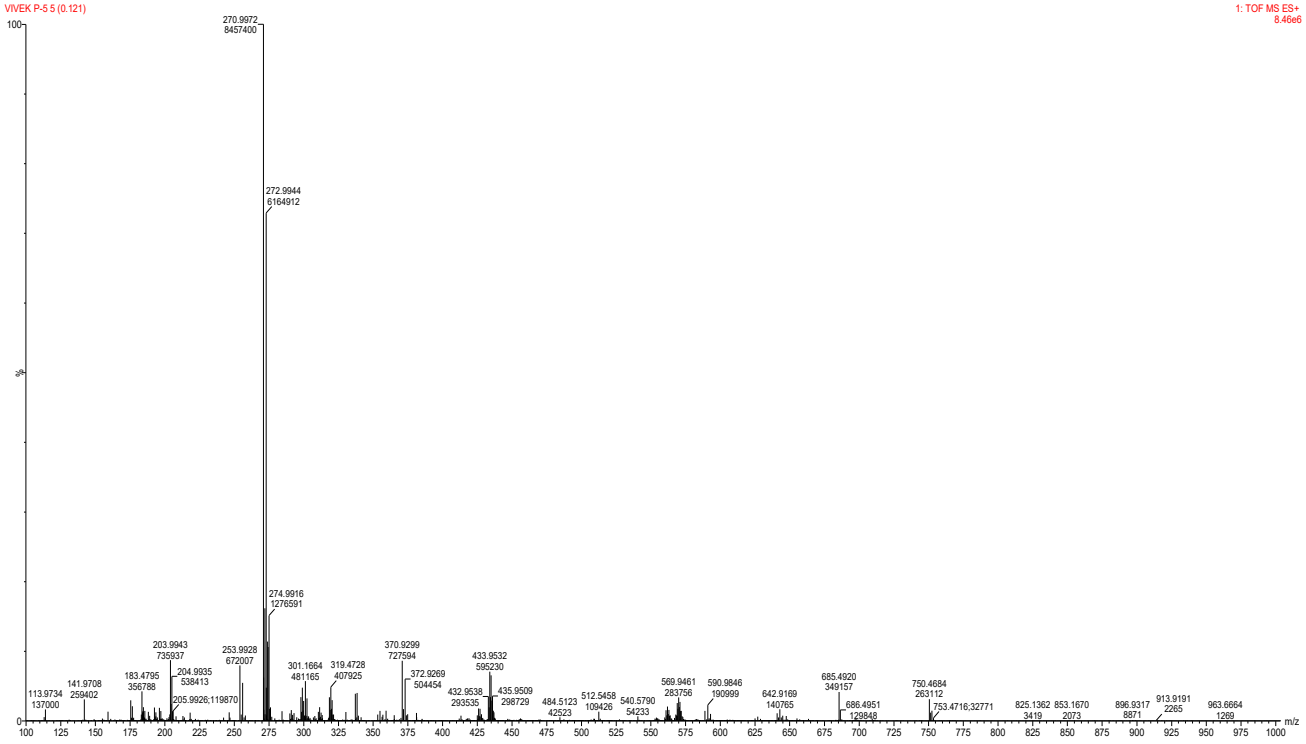

Figure 12a: Mass spectrum of bis (4-chlorophenyl) sulfoxide.

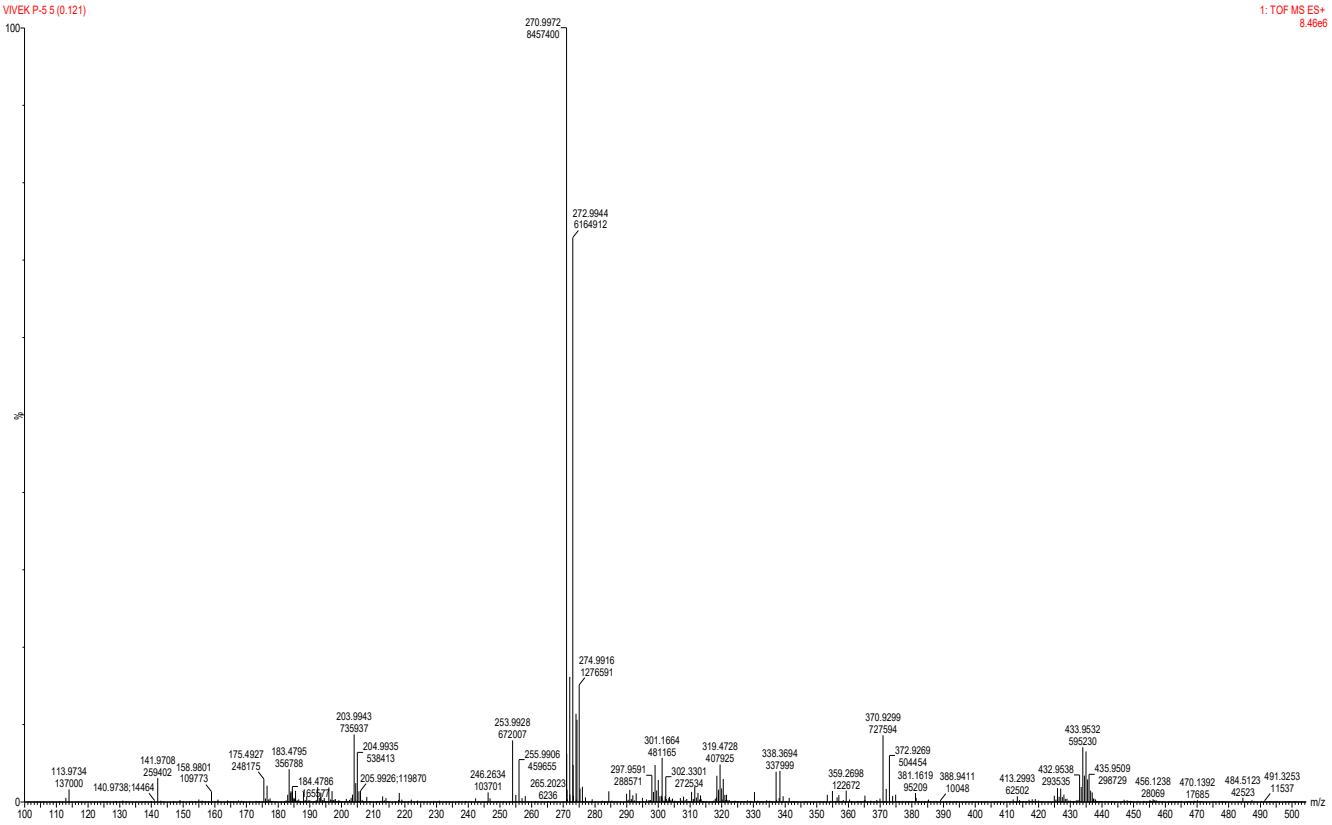

Figure 12b: Mass spectrum of bis (4-chlorophenyl) sulfoxide (expended form).

12. Zeta potential analysis

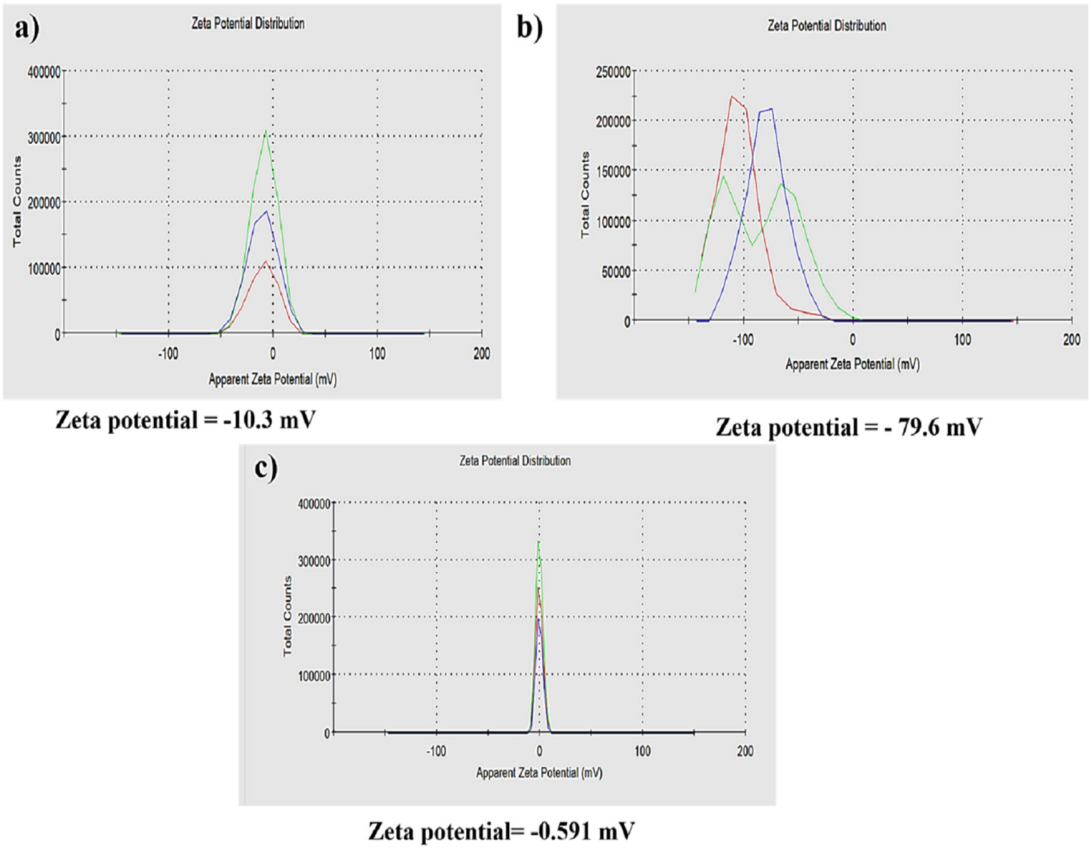

Figure S13. Zeta potential analysis of (a) Eosin-Y with the value of -10.3mV, (b) EY-S-g-C_3N_4 photocatalyst with -79.6mV, and (c) thiourea with -0.591 mV.

13. Particle size studies

Dynamic light scattering (DLS) techniques were investigating the average particle size of eosin-Y, thiourea and EY-S-g-C_3N_4 photocatalyst in solution phase with the help of nano-zetasizer (NZS90). The average particle size of EY-S-g-C_3N_4 photocatalyst (near about 500 nm) is smaller than eosin-Y (~750 nm) and thiourea (~5500 nm) as shown in Figure S11. As per reported method,[3,4] smaller size of photocatalyst is highly efficient than the bigger size of photocatalyst due charge carrier excitation and surface-active sites. Therefore, newly designed EY-S-g-C_3N_4 photocatalyst is more efficient than eosin-Y and thiourea.

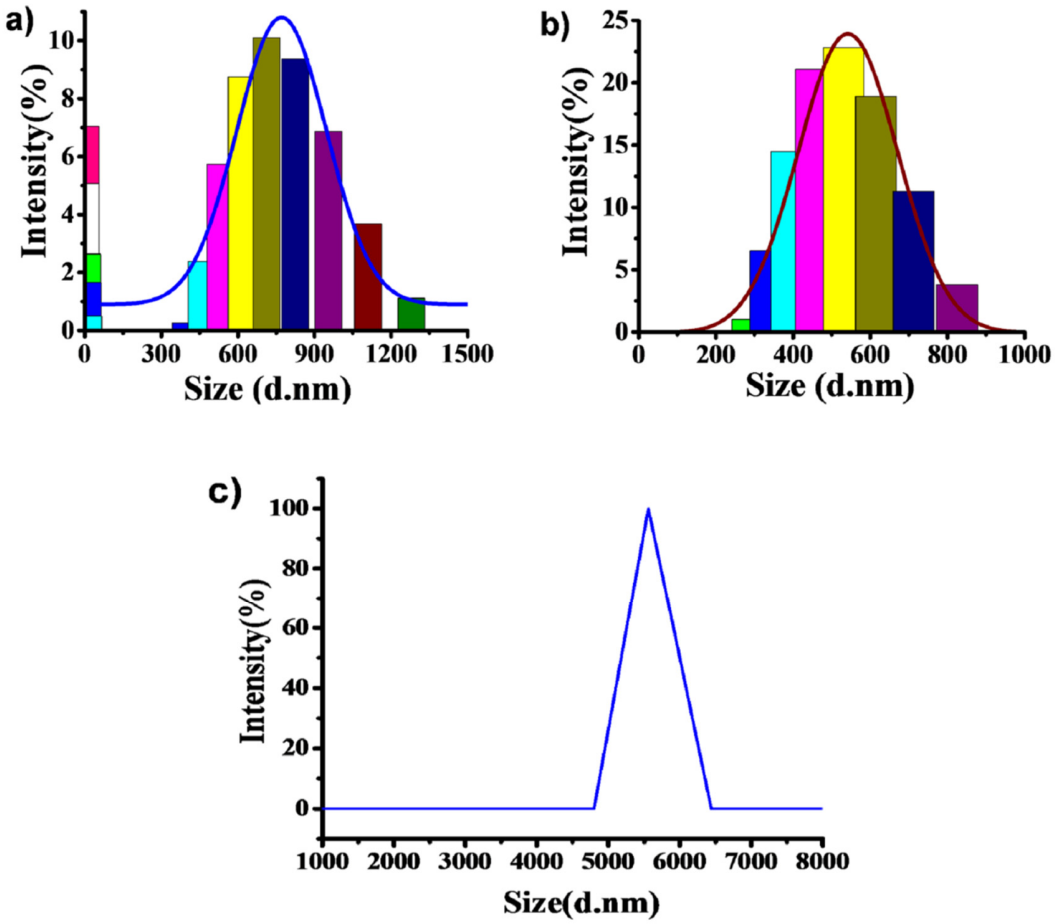

Figure S14. Particle size analysis of (a) Eosin-Y, (b) EY-S-g-C_3N_4 photocatalyst, and (c) thiourea.

14. Control experiment in the absence of NAD^+

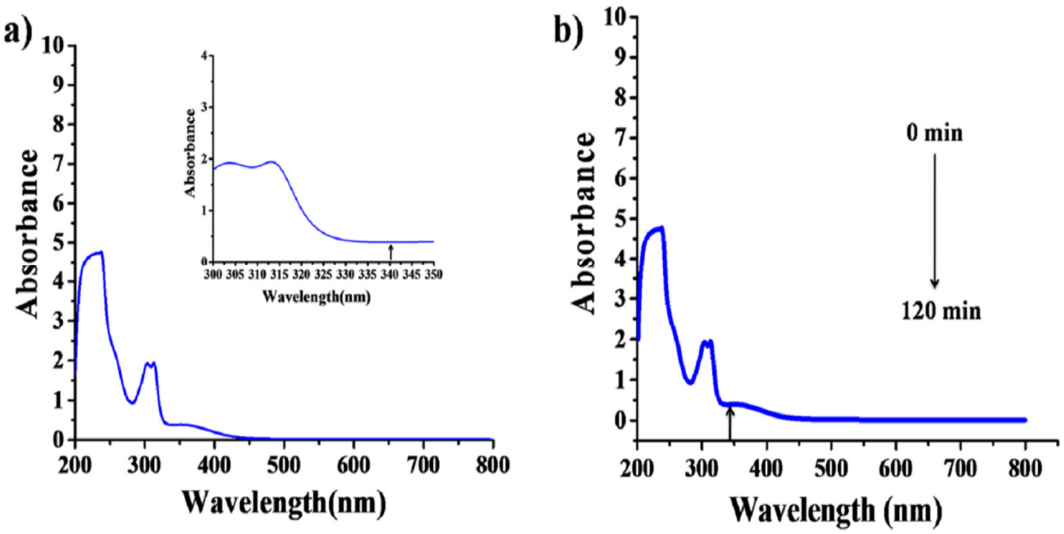

Figure S15. Control experiment for NADH regeneration in absence of NAD^+ under solar light, no absorption peak obtained at 340 nm (b) Control experiment for NADH regeneration in absence of NAD^+ under solar light, no absorption peak obtained at 340 nm in different time interval.

15. XRD and XPS studies

The XRD patterns of EY-S-g-C_3N_4 photocatalyst and reuse EY-S-g-C_3N_4 photocatalyst are shown in Figure S15. The characteristic peak of EY and S-doped g-C_3N_4 observed at 10.41° and 27.8° which is clearly indicate the existence of EY and sulfur, respectively.[7-9] Furthermore, XRD pattern of reused EY-S-g-C_3N_4 photocatalyst still reveals the same characteristic peaks. These results clearly indicate that the EY-S-g-C_3N_4 photocatalyst is highly stable, therefore not losses the photocatalytic properties during regeneration of NADH\NADPH and oxidation of bis(4-chlorophenyl) sulfide to bis(4-chlorophenyl) sulfoxide. Stability of photocatalyst also confirmed by X-ray photoelectron spectroscopy (XPS) analysis.

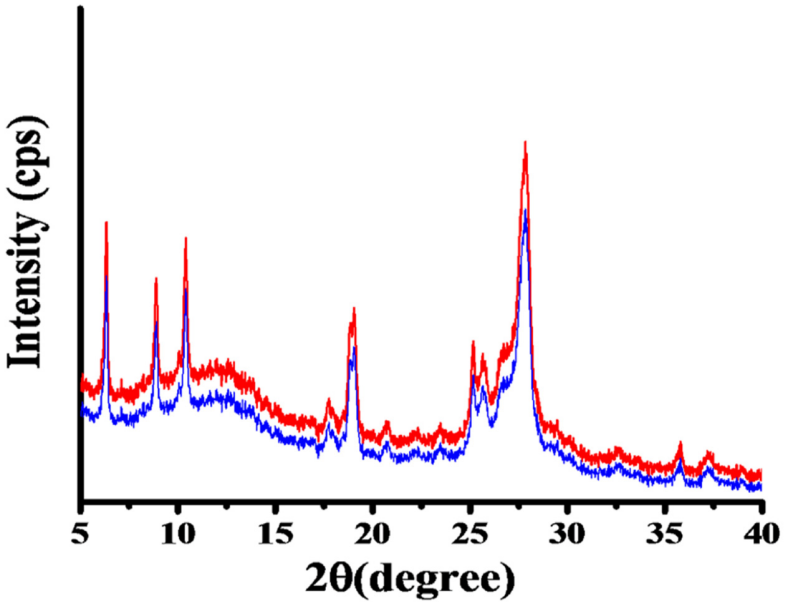

Figure S16. XRD spectra of fresh EY-S-g-C_3N_4 photocatalyst (red line) and reused EY-S-g-C_3N_4 photocatalyst (blue line).

The restoration of EY-S-g-C_3N_4 was confirmed by XPS (Model: KARTOS AXIS NOVA). The XPS spectrum of EY-S-g-C_3N_4, the intensity of carbon 'C'1s (Figure S16b) can be attributed three peaks at 283.8 eV (C-C), 284.9 eV (C=N) and 287.9 eV (N-C=N).[10]The spectra of N 1s (Figure S16c) is allocated peak near about at 397.9 eV for nitrogen (N) bonded with two carbon (C=N-C) in an aromatic triazine rings, and the additional peak near about at 401.0 eV sp^3-hybridized nitrogen (N-H) of g-C_3N_4 rings, i.e. heptazine rings.[11] In addition, the spectra of 'O' 1s (Figure S16d) is designated peak at 529.9 eV after the formation of EY-S-g-C_3N_4 composite indicated the presence of C=O bond along with C-N bond (from N1s peaks).[12]Furthermore, two peaks near about at 160.9 eV and 163.8 eV in S2p spectra (Figure 16e) assigned the binding energy of S^{2-} and N-S bond, which indicates the existence of Sulfur in g-C_3N_4.[13] Moreover, as shown in Figure S16f the XPS spectra of Br 3d which attributed two peak at binding energy 68.9 eV, 70.3 eV corresponding to Br of eosin-Y.[8]Additionally, the spectrum (Figure S16a) of EY-S-g-C_3N_4, the intensity of the carbon 'C' 1s peak relative to the nitrogen 'N' 1s peak was reduced with the finding of the oxygen 'O' 1s peak along with Br 3d, and S2p in the XPS survey. This confirmed the creation of an amide bond in place of the carboxyl group and also confirmed the S-doped in g-C_3N_4.[10] Finally, the experimental results revealed the formation of EY-S-g-C_3N_4 composite as a photocatalyst.

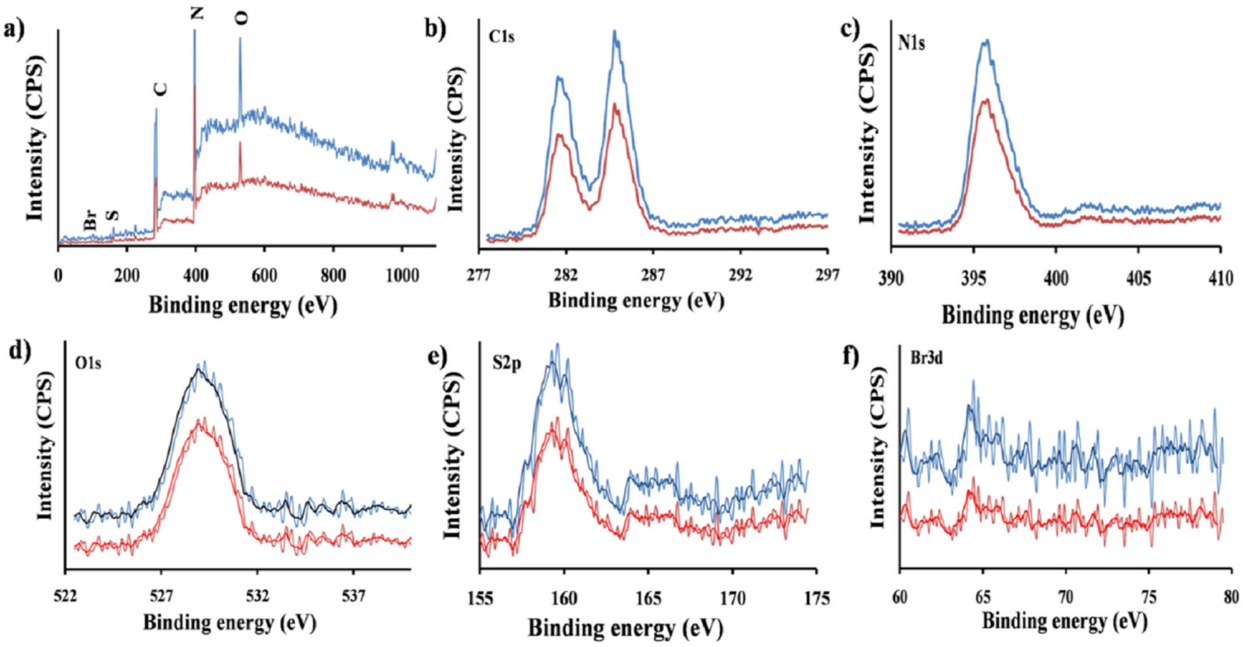

Figure S17. XPS spectra of fresh EY-S-g-C_3N_4 (blue line) and reused EY-S-g-C_3N_4 (red line) photocatalyst. (a) XPS survey spectra of EY-S-g-C_3N_4 and (b, c, d, e, f) C1s, N1s, O1s, S2p, Br3d high resolution XPS spectra of EY-S-g-C_3N_4.

16. References

1. Y. Wang, Yu. Tian, Li. Yan and Z. Su, *J. Phys. Chem. C,* 2018, **122**, 7712–7719.
2. M. J. Frisch, G. W. Trucks, H. B. Schlegel, G. E. Scuseria, M. A. Robb, J. R. Cheeseman, G. Scalmani, V. Barone, G. A. Petersson and H. Nakatsuji, et al. Gaussian 16 Rev. B.01; Wallingford, CT, 2016.
3. B. Kumru, M. Antonietti and B. V. K. J. Schmidt, *Langmuir,* 2017, **33**, 9897–9906.
4. S. J. Hong, H. Jun, P. H. Borse and J. S. Lee, *Int. J. Hydrog. Energy,* 2009, **34**, 3234-3242.
5. S. Cao, J. Low, J. Yu and M. Jaroniec, *Adv. Mater.*2015, **27**, 2150–2176.
6. H. Zhang, J. Lin, Z. Li, T. Li, X. Jia, X.-L. Wu, S. Hu, H. Lin, J. Chen and J. Zhu, *Catal. Sci. Technol.* 2019, **9**, 502-508.
7. L. Jiang, X. Yuan, G. Zeng, X. Chen, Z. Wu, J. Liang, J. Zhang, H. Wang and H. Wang, *ACS Sustainable Chem. Eng.,* 2017, **5**, 5831-5841.
8. B. Li, Y. Zhanga, F. Duanmua, Y. Shena, Z. Shena and S. Zhong, *Photochem. Photobiol. Sci.*, 2019, **18***,* 1408-1418.
9. M. Pudukudy, Q. Jia, Y. Dong, Z. Yue and S. Shan, *RSC Adv.,*2019, **9**, 32517-32534.
10. H. J. Kong, D. H. Won, J. Kim, and S. I. Woo, *Chem. Mater.,* 2016, **28**, 1318−1324.
11. W. Chen, T.-Y. Liu, T. Huang, X.-H. Liu and X.-J. Yang, *Nanoscale,* 2016, **8**, 3711−3719.
12. R. K. Yadav, J.-O. Baeg, A. Kumar, K.-j. Kong, G. H. Oh and N.-J. Park, *J. Mater. Chem. A,* 2014, **2**, 5068-5076.
13. Y. Chang, F. Hong, C. He, Q. Zhang and J. Liu, *Adv. Mater.,* 2013, **25**, 4794−4799.